Arabian Journal of Chemistry (2020) 13, 3558–3570

King Saud University

Arabian Journal of Chemistry

www.ksu.edu.sa
www.sciencedirect.com

ORIGINAL ARTICLE

Facile fabrication of superhydrophobic and superoleophilic green ceramic hollow fiber membrane derived from waste sugarcane bagasse ash for oil/water separation

Mohd Riduan Jamalludin [a,b], Siti Khadijah Hubadillah [c], Zawati Harun [b,*], Mohd Hafiz Dzarfan Othman [c], Muhamad Zaini Yunos [b], Ahmad Fauzi Ismail [c], Wan Norharyati Wan Salleh [c]

[a] *Faculty of Engineering Technology, Universiti Malaysia Perlis (UniMAP), Kampus UniCITI Alam, Sungai Chuchuh, Padang Besar 02100, Perlis, Malaysia*
[b] *Advanced Materials and Manufacturing Centre (AMMC), Faculty of Mechanical and Manufacturing Engineering, Universiti Tun Hussein Onn Malaysia, 86400 Parit Raja, Batu Pahat, Johor Darul Takzim, Malaysia*
[c] *Advanced Membrane Technology Research Centre (AMTEC), Faculty of Chemical and Energy Engineering, Universiti Teknologi Malaysia, 81310 Skudai, Johor, Malaysia*

Received 28 September 2018; accepted 12 December 2018
Available online 31 December 2018

KEYWORDS

Ceramic membrane;
Sugarcane bagasse waste;
Oil/water separation;
Sol-gel;
TEOS

Abstract Green ceramic hollow fiber membranes with superhydrophobic and superoleophilic surfaces (ss-CHFM/WSBA) were successfully fabricated via facile sol–gel process using tetraethoxysilane (TEOS) and methyltriethoxysilane (MTES) as precursors. In this work, silica solution was prepared using the modified Stöber method. This process was followed by dipping the pristine membranes into the sol–gel solution at various grafting times (0–90 min), grafting cycles (0–4 cycles), and calcination temperatures (400–600 °C). The wettability, surface morphology, and chemical composition of the pristine and ss-CHFM/WSBA membranes were investigated. The results showed that increasing the grafting time has increased the wettability of ss-CHFM/WSBA with high contact angle of up to 163.9°. Similarly, increasing grafting cycle has enhanced the hydrophobicity of ss-CHFM/WSBA due to the formation of hierarchical structure of grafting cycle which were more than one. The optimum calcination temperature for ss-CHFM/WSBA was identified. It was found that increasing the calcination temperature has degraded the sol template on the sur-

* Corresponding author.
E-mail address: zawati@uthm.edu.my (Z. Harun).
Peer review under responsibility of King Saud University.

ELSEVIER Production and hosting by Elsevier

https://doi.org/10.1016/j.arabjc.2018.12.007

face of ss-CHFM/WSBA, hence decreasing the wettability. The preliminary performance tests showed that ss-CHFM/WSBA grafted at 60 min, 3 cycles, and calcined at 400 °C showed excellent oil/water separation efficiency of 99.9% and oil flux of 137.2 L/m^{2}h.

1. Introduction

Oily wastewater is generated by various industrial processes such as petroleum industries, chemical and petrochemical plants, oil refineries terminal during washing of reserving tank, and metal working plants. This type of pollution can affect groundwater, seawater, crop production drinking water as a result of the percolation of contaminants in produced water into the water resources, endangering aquatic resources, atmospheric pollution, destructing the natural landscape, and arising safety concern due to oil burner coalescence. The generated water effluent often contains micrometer-sized oil droplets dispersed in water, forming a stable oil-in-water emulsion even without any stabilizer (Yu et al., 2017). Oil is an organic matter and important contaminant in wastewater that affects the environment severely (Zhou and Wu, 2015; Hubadillah et al., 2018). It was reported that more than 2000 million tons of wastewater produced by oil refineries in the world (Zuo et al., 2009). The conventional methods such as gravity separation, adsorption, oil skimmers, biological treatment, and sedimentation in a centrifugal field have been applied in oily wastewater treatment (Vinoth Kumar et al., 2015). However, these conventional methods have disadvantages in terms of low efficiency, high operation costs, corrosion, and recontamination problems. For instance, the method of using oil skimmers contaminates the environment easily and the method of combustion also results in secondary pollution of water (Song et al., 2017).

In recent years, with the in-depth studies of superhydrophobic and superoleophilic surfaces, researchers have started to explore materials and design coatings to fabricate oil/water separation surfaces with special wettability. In 2004, Feng et al. coated copper mesh with polytetrafluoroethylene (PTFE) to fabricate a mesh for oil/water separation (Feng et al., 2004). Consequently, a lot of methods have been explored to solve the oil/water separation problem, for example, template method (Feng and Jiang, 2006), sol–gel process (Yang et al., 2010), chemical etching (Guo et al., 2014); electrospinning (Li et al., 2016; Ge et al., 2017), and chemical vapor method (Crick et al., 2013; Zhang and Seeger, 2011). Herein, copper meshes are widely chosen by researchers as a support meshes for oil or water separation because of its availability, low cost, and its porous structure. Unfortunately, one of the most serious bottleneck of copper mesh is its susceptibility to corrosion, that is, oxidation (Hedin et al., 2018), resulting in a shorter lifespan. Therefore, nonmetallic substrates such as sponges and textiles were chosen, replacing the copper mesh. For example, melamine sponges were used as the core material for preparing porous materials possessing superhydrophobic and superoleophilic property for continuous separation of oils and organic solvents from water (Gupta et al., 2016). Zhang et al. fabricated smart textiles with switchable superoleophobicity by grafting a block copolymer comprising pH-responsive poly(2-vinylpyridine) and oleophilic/hydrophobic polydimethylsiloxane blocks on these materials (Zhang et al., 2012). Unfortunately, most sponges and textile fibers became completely rotten in 3–5 weeks. Therefore, recent studies have been focusing on the stainless steel mesh as superhydrophobic and superoleophilic substrates for oily wastewater separation (Li et al., 2015; Liu et al., 2016; Wen et al., 2018). Because of the unique ability of stainless steel to resist corrosion, heat damage, and chemical damage, high strength duplex grades provide an added strength, allowing for a reduced thickness in the material, providing a high upfront cost than that of the other types of substrates.

Membrane technologies are more favorable as substrates as they are cost-effective and fast, highly selective, and flexible to be integrated with other processes (Jamalludin et al., 2016). Many approaches were taken by researchers in the utilization of membrane as a support for water treatment application. Among all the membrane types, ceramic membranes present interesting advantages such as high thermal and chemical stability, high surface area, and extended lifetime in oily wastewater treatment (Kingsbury and Li, 2009). Many researchers reported that most of the ceramic membranes are fabricated from particles of ceramic oxides such as Al_2O_3, TiO_2, ZrO_2, and SiO_2 (Obada et al., 2016; Koonaphapdeelert and Li, 2007; Harun et al., 2014; Hubadillah et al., 2018). The early research in ceramic membrane fabrication focused towards the utilization of an expensive precursor, α-alumina, to fabricate the membrane (Yang et al., 2011). In addition, alumina has been widely used in ceramic membrane fabrication towards various separation technologies due to the considerable attention received for its usage in separation processes because of its thermal, chemical, and mechanical stabilities (Kingsbury and Li, 2009). However, alumina membrane is considered to be costly. It was reported that alumina membrane costed around \$1200–\$2000/m^2 which is more than half the price of polymeric membranes (Obada et al., 2016). Still, ceramic membrane is in high consideration when it comes to other advantages.

Nowadays, alternative ceramic material like clay, dolomite, apatite, fly ash, natural raw clay, and kaolin which are categorized as cheap raw materials have been used in the ceramic membrane fabrication to reduce the production cost (Yang et al., 2011; Hubadillah et al., 2016; Hubadillah et al., 2018). Interestingly, recent research is oriented to the use of agricultural waste such as fly ash and rice husk ash for the fabrication of green ceramic membrane (Hubadillah et al., 2016; Dong et al., 2008). Notably, most agricultural waste has been converted into ashes through calcination process and disposed of in landfills. However, the increasing refusal of communities to have landfills nearby, as well as the increased pressure from the environmental agencies for proper waste management is creating the needs for alternative final disposal, consistent with the environmental needs at a rational cost (Martínez et al., 2012). In fact, utilization of ashes from agricultural waste for

energy production, alternative materials replacing cement, and extraction of silica have become increasingly important. In our previous work, green ceramic hollow fiber membrane derived from waste sugarcane bagasse ash was successfully prepared via phase inversion and sintering technique and showed interesting potential to act as a membrane support (Jamalludin et al., 2018). Therefore, the aim of this study is to fabricate the superhydrophobic and superoleophilic green ceramic hollow fiber membrane (ss-CHFM/WSBA) through sol–gel grafting for oil/water separation. To evaluate the prepared ss-CHFM/WSBA, three grafting parameters (grafting time, grafting cycle, and calcination temperature) were studied and the results were characterized in terms of morphology, wettability properties, and oil/water separation.

2. Experimental section

2.1. Materials

Green ceramic hollow fiber membranes with pore sizes of 75 mm were from our previous study (Jamalludin et al., 2018). Tetraethyl orthosilicate (TEOS), methyltriethoxysilane (MTES), ammonia (NH_3, 25%, A.R.), absolute ethanol (EtOH, 99.5%, A.R.), and distilled water (H_2O) were used without any further purification.

2.2. Preparation of silica sol

The silica sol was prepared via the modified Stöber method. Firstly, 0.4 mol of TEOS, 1.04 mol of NH_3, 3.55 mol of H_2O, 0.2 mol of MTES, and 13.92 mol of ethanol were mixed for 90 min at 30 °C to obtain the silica sol. The silica sol was aged at room temperature for 7 days before being used. A porous ceramic tube was immersed in the silica sol for 2 h at room temperature and then dried at 110 °C for 30 min. This procedure was repeated for three times. After that, the tube was annealed at 400 °C for 4 h.

2.3. Fabrication of superhydrophobic and superoleophilic green ceramic hollow fiber membranes

Dip-coating method (Dip coater: PTL-MM01, Canada) was used for the fabrication of superhydrophobic and superoleophilic green ceramic hollow fiber membranes (ss-CHFM/WSBA) with a withdraw speed of 10 mm/min. Prior to the dip-coating process, all membranes were rinsed with ethanol and dried in an oven at 100 °C for 24 h to enhance the OH bonding on the membrane surface. Afterwards, the membranes were dipped into the sol solutions at various grafting times (0–90 min), grafting cycles (0–4 cycles), and calcination temperatures (400–600 °C). The grafting mechanism of ss-CHFM/WSBA is shown in Fig. 1.

2.4. Membrane characterization

Scanning electron microscopy (SEM, model JSM 6380LA) was used to observe the surface morphology of the membrane. The membrane sample was mounted horizontally and coated with gold–palladium using a sputter coater to make it becomes conductive. The observations were carried out on the cross section and upper surface of the hollow fiber ceramic membrane.

The superhydrophobicity and superoleophilic properties of hollow fiber ceramic membrane was determined via contact angle measurement. The sessile drop technique method with static contact angle measurement was carried out using a contact angle goniometer (OCA 15 plus). The image of the small water droplet on membrane surface was captured within 1 s. To minimize the experimental error, the contact angles were measured at 10 difference points for each sample and the average was reported with the standard deviation value.

Fourier transform infrared spectroscopy (FTIR: Spectrum 100, PerkinElmer, Waltham, MA) was used to study qualitatively the methyl groups grafted on the ss-CHFM/WSBA. The FTIR was performed at resolution of 5 cm^{-1} and scan number of 5.

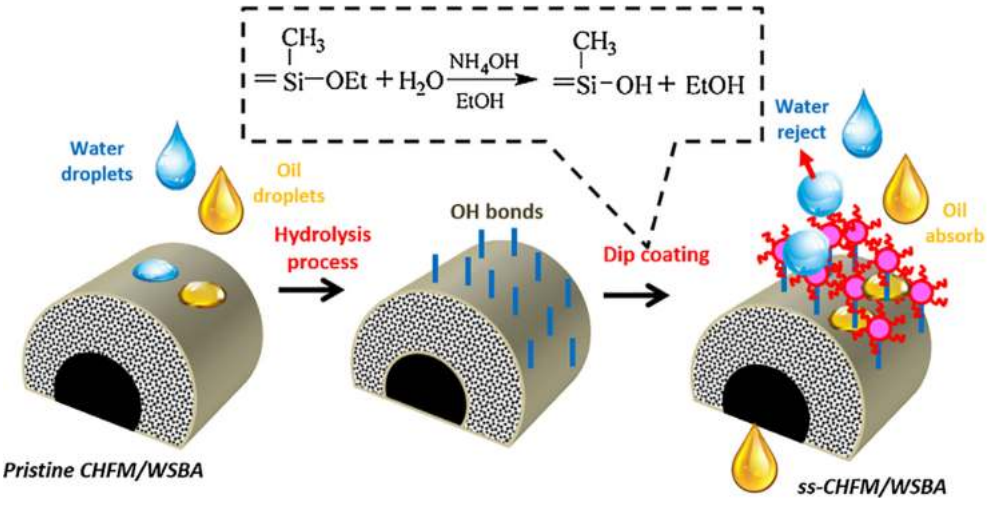

Fig. 1 Grafting mechanism of ss-CHFM/WSBA through dip-coating process.

2.5. Oil/water separation

A dead-end filtration system as shown in Fig. 2 was used for water flux and oily wastewater separation. The oil flux (J) measurement was carried out at 1 bar and was determined using the following equation:

$$J = \frac{V}{A \times t}$$

where V (L) is the volume of permeated water, A (m^2) is the valid area of the membrane, and t (s) is the permeation time.

Water content analysis was performed based on ASTM D 2709. The volume of oil sample was first measured and then heated in an oven for approximately 10 min. The moisture content of oil was measured using a moisture analyzer. The oil was placed in the weighing tray in the moisture analyzer. The process started with heating for 1 min 21 s at a temperature of about 97–100 °C. Consequently, the oil separation efficiency (R) was calculated using the following equation:

$$R(\%) = \frac{C_f - C_p}{C_p} \times 100$$

where C_f is the oil concentration in the feed stream and C_p is the oil concentration in the permeate stream. The concentration of oily wastewater was determined by measuring the absorbance of the oily wastewater before and after microfiltration using a UV–visible spectrophotometer (Thermo Scientific, Genesys 10S) at a wavelength of 254 nm.

3. Results and discussion

3.1. Effect of grafting time

The surface morphologies of superhydrophobic and superoleophilic green ceramic hollow fiber membranes (ss-CHFM/WSBA) prepared at different grafting times ranging from 0 to 90 min, 2 cycles of grafting, and calcined at 400 °C were observed through SEM and the images are displayed in Fig. 3. The pristine CHFM/WSBA showed a porous worm-like pores structure with a large pore of 1.85 μm. The detailed information on the formation of worm-like pores is described elsewhere (Jamalludin et al., 2018). These pores are slightly smaller than the pores of stainless steel that was used as the substrate for oil-in-water separation in the literatures (100–200 μm) (Liu et al., 2016; Xiang et al., 2018).

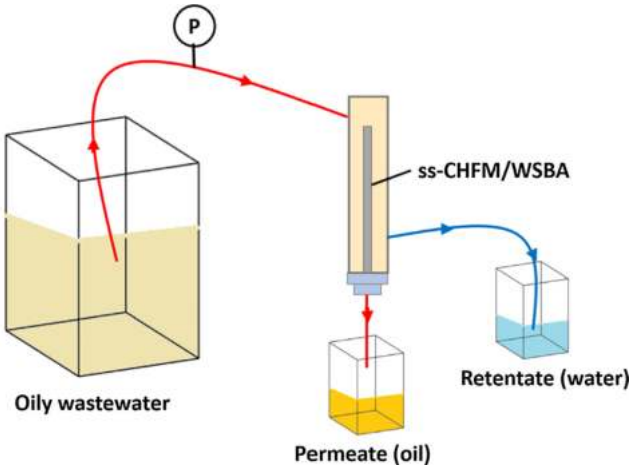

Fig. 2 Laboratory setup for oily wastewater separation.

At the grafting time of 30 min, the surface of ss-CHFM/WSBA were covered by nano-silica particles without disturbing the membrane pores. However, the nano-silica particles started to attach on the wall of the membrane pores when the grafting time was increased to 60 min. Surprisingly, the grafting time of 90 min led to totally blocked pores with nano-silica and reduced the number of pores on the ss-CHFM/WSBA surface (Fig. 3, D1 and D2). In addition, the SiO_2 particles were entangled with each other. These findings show that an increase of grafting time leads to a change in the morphology of ss-CHFM/WSBA and the formation of nano-silica as a result from the reaction between SiO_2 and substrate during sol–gel grafting process. A similar trend was also observed for the case of stainless steel as substrate (Liu et al., 2016).

In addition, it is interesting to highlight the increment of Si mass measured from EDX (Fig. 3, A3–D3). For pristine CHFM/WSBA, the Si mass was 7.97% indicating that the CHFM/WSBA itself contain Si. After grafting process at 30 min, the Si mass increased from 7.97% to 12.32%. Further increment to 13.87–20.42% of Si was observed when the grafting time was increased to 60 and 90 min, respectively. To support the EDX result, the weight of pristine CHFM/WSBA with a length of about 5 cm was weighed, as shown in Fig. 4. The similar CHFM/WSBA was subjected to the grafting process at various grafting times. Interestingly, the weight of the grafted ss-CHFM/WSBA increased with increasing grafting time, in which in line with the SEM and EDX results.

As stated by Chen et al., sol–gel solution that made up from TEOS and MTES contains an abundance of —OH groups (Chen et al., 2011). Subsequently, the —OH groups will react with the —OH on the substrate surface to convert a major amount of the —OH groups to —Si(CH_3) (Hubadillah et al., 2020). Specifically, the amount of nano-silica formation on the membrane surface depends on grafting time. Also, it is interesting to mention that the substrate used in this study do not need any preliminary treatment such as alcohol treatment to improve its affinity for SiO_2 sol–gel to react because ceramic membrane is hydrophilic in nature and induces natural —OH bonds (Hubadillah et al., 2020). As mentioned previously in our earlier work (Jamalludin et al., 2018), the mixture composition of WSBA with high percentage of silica will not only able to increase strong affinity of SiO_2 sol–gel reaction but other composition such as alumina in WBSA also able to increase the hydrophobicity of grafted membrane. Thus, it is concluded that WBSA may not only able to provide superhydrophilic property, but its mixture composition makes them easier to be converted into superhydrophobic and superoleophilic properties.

To determine the superhydrophobicity of ss-CHFM/WSBA, water contact angle values for pristine CHFM/WSBA and grafted ss-CHFM/WSBA prepared at different grafting times were measured (Fig. 5). As expected, no contact angle value can be measured for the pristine CHFM/WSBA as it is difficult to get static water droplet on the membrane surface, as presented in Fig. 6. Whereas, Fig. 7 illustrates the images of water and oil droplet on the pristine CHFM/WSBA and grafted ss-CHFM/WSBA. The water droplet from the syringe immediately immersed into the pristine CHFM/WSBA.

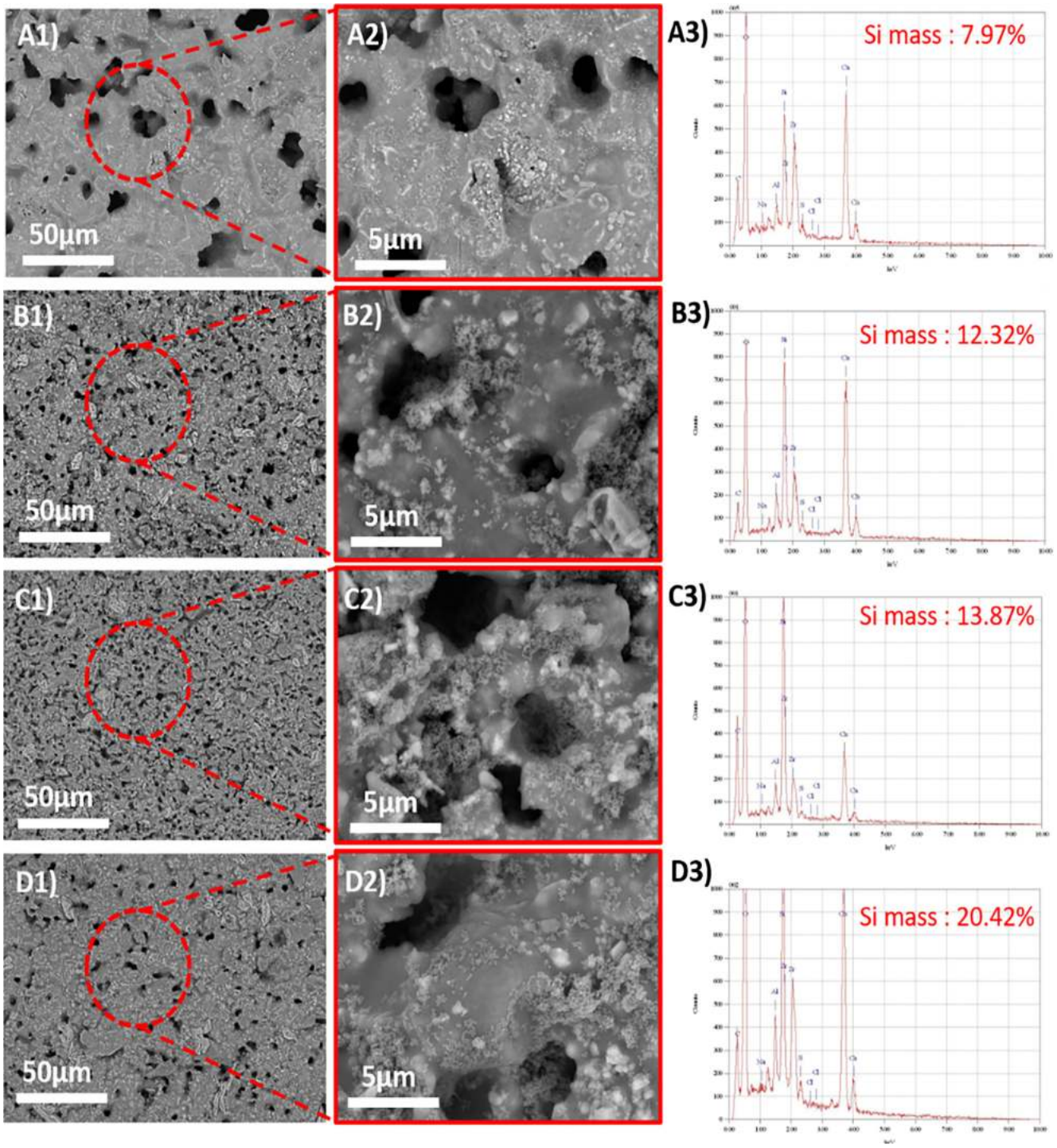

Fig. 3 SEM images of superhydrophobic and superoleophilic CHFM/WSBA grafted at (a) 0 min, (b) 30 min, (c) 60 min, and (d) 90 min at (1) 1000× and (2) 10,000× magnifications.

There are two observation can be made here: (1) the pristine CHFM/WSBA possessed hydrophilicity behavior (Hubadillah et al., 2017) and (2) the larger pores of CHFM/WSBA trapped the water droplet into the pores like sponge. As expected, the contact angle values for ss-CHFM/WSBA prepared at different grafting times of 30, 60, and 90 min were 154.3°, 161.1°, and 163.9°, respectively. Remarkably, these values showed that all ss-CHFM/WSBA possessed superhydrophobicity properties by having a contact angle value of more than 150°. According to Tuteja et al., superhydrophobic surfaces display water contact angles of more than 150° in conjunction with low contact angle hysteresis (Tuteja et al., 2008). In addition, the contact angle values of ss-CHFM/WSBA were measured using sessile drops of crude oil. Interestingly, the value of contact angle with oil on ss-CHFM/WSBA was consistent with the value of contact angle with water on pristine CHFM/

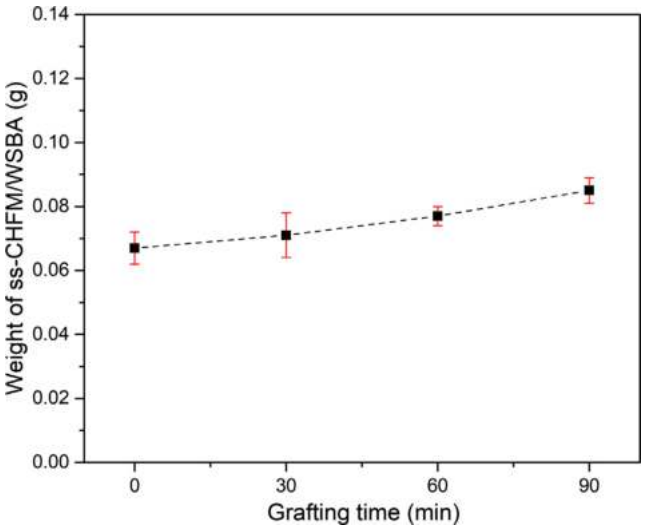

Fig. 4 Weights of pristine CHFM/WSBA and grafted ss-CHFM/WSBA prepared at different grafting times.

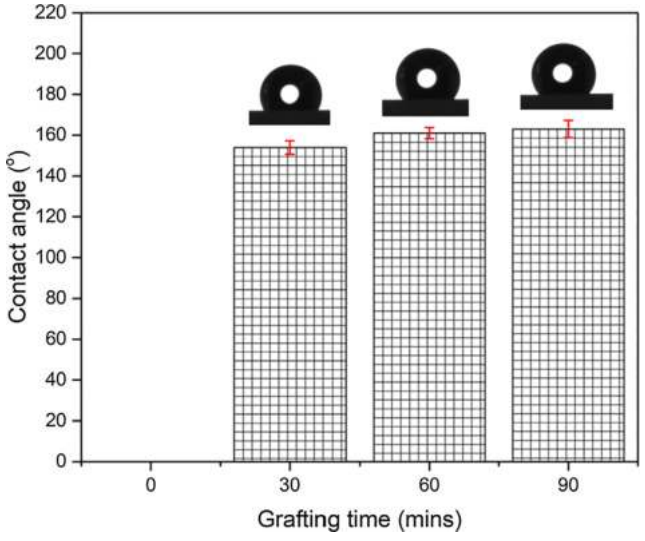

Fig. 5 Contact angle values of ss-CHFM/WSBA prepared at different grafting times.

WSBA, which was 0° (Fig. 8). Due to this, it is proven that the ss-CHFM/WSBA in this study induced superhydrophobic and superoleophilic properties.

Fig. 9 presents the performance of ss-CHFM/WSBA prepared at different grafting times towards the oil flux and oil separation efficiency of synthetic oil wastewater at 1000 ppm. Increasing the grafting time from 30 to 90 min reduced the oil flux, whereas the opposite was observed for the oil separation efficiency. Herein, ss-CHFM/WSBA grafted for 30 min had the highest oil flux (151.3 L/m^{2}h), followed by ss-CHFM/WSBA grafted at 60 min (135.7 L/m^{2}h) and 90 min (51.6 L/m^{2}h). Meanwhile, the oil separation efficiency for the pristine membrane was 5.9%. This value increased to 84.2%, 97.2%, and 98.9% for ss-CHFM/WSBA grafted at 30, 60, and 90 min. These oil separation efficiency values describe the ability of membrane to attract and permeate more oil than water from the feed concentration. Therefore, as the grafting time and hydrophobicity value increased, the permeate flux was decreased due to less water concentration. Therefore, the highest oil flux of 226.7 L/m^{2}h was reported for pristine membrane, however, the mixture of oil and water was filtered together instead of oil only from the synthetic wastewater. This explained the reason for the low separation efficiency.

According to Lai et al. (2018), when superoleophilic and superhydrophobic coatings are introduced on porous substrate, only oil will go through the substrate and water will remain on the other side (Lai et al., 2018). Subsequently, hybrid application of oil adsorption and separation can be done in a single step. Unfortunately, data on oil flux separation is rarely reported. In view of this, this study discusses the trend of oil separation as well as oil separation efficiency. For example, Song et al. fabricated superoleophilic and superhydrophobic copper mesh for oil/water separation and obtained a high separation efficiency of 92% for various oils but no oil flux was recorded.

3.2. Effect of grafting cycle

In the previous section, we prepared ss-CHFM/WSBA at different grafting times, 2 grafting cycles, and calcined at 400 °C. Based on the morphological study and performance of ss-CHFM/WSBA prepared at different grafting times towards oil separation, it was found that grafting times of 60 min was the best due to high oil flux and oil separation efficiency. However, the distribution of nano-silica particles on the surface of

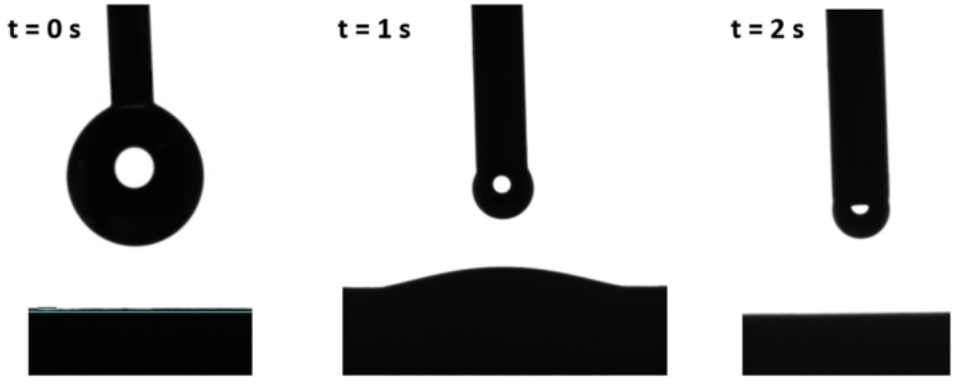

Fig. 6 Images of water droplet on pristine CHFM/WSBA at different times.

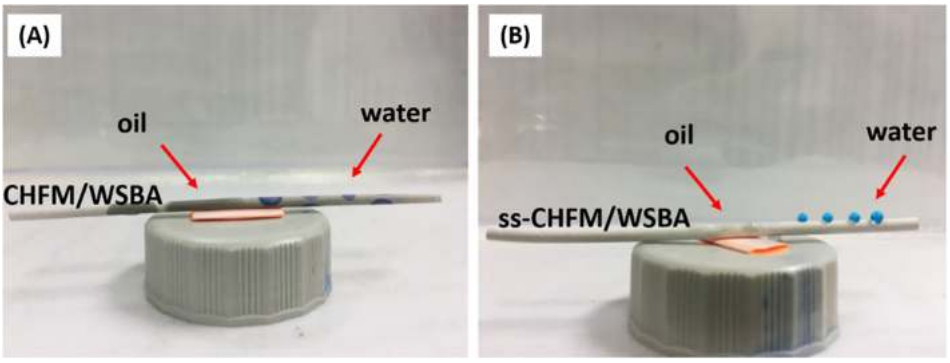

Fig. 7 Images of water and oil droplets on (a) pristine CHFM/WSBA and (b) grafted ss-CHFM/WSBA.

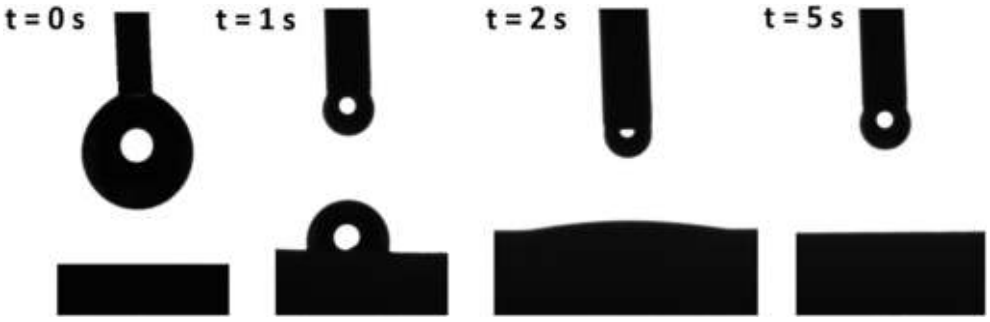

Fig. 8 Images of oil droplet on grafted ss-CHFM/WSBA at different times.

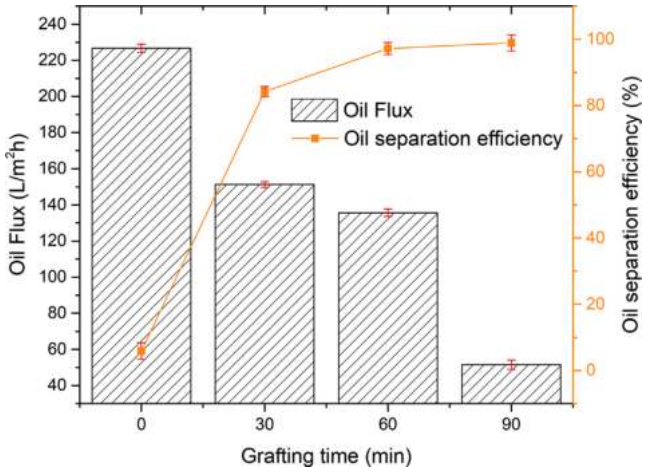

Fig. 9 Performance of ss-CHFM/WSBA prepared at different grafting times towards oil separation.

ss-CHFM/WSBA was uneven. Accordingly, the effects of grafting cycle ranging from 0 to 4 cycles were investigated and the SEM images are presented in Fig. 10. Fig. 10 (A1 and A2) show the surface of the pristine CHFM/WSBA that consist worm-like pores as discussed in our previous work (Jamalludin et al., 2018). For grafting cycle of 1, the nano-silica particles started to form on the surface of ss-CHFM/WSBA but the distribution was obviously uneven. Increasing the grafting cycle to 2 cycles increased the number of nano-silica particles that were distributed evenly on the surface of ss-CHFM/WSBA. The increment of Si mass (Fig. 10 [A3–E3]) and ss-CHFM weight (Fig. 11) are in line with the SEM images.

However, it was obvious that the distribution was not uniform when observed in high magnification. In particular, there were some areas on the ss-CHFM/WSBA surface that were not covered by nano-silica particles especially around the ss-CHFM/WSBA pores. In this case, no —OH bonds existed on the ss-CHFM/WSBA pores which decreased the reaction between —OH bonds from the sol–gel solution and —OH on the substrate. Consequently, the nano-silica particles were distributed evenly on the ss-CHFM/WSBA surface when grafting for 3 and 4 cycles. In fact, most of the ss-CHFM/WSBA pores were covered by the nano-silica particles. At high magnification, it was revealed that the nano-silica particles were agglomerated when 4 cycles of grafting were applied. This phenomenon was also observed by Yang et al. which also applied 4 cycles of grafting on the stainless steel mesh (Yang et al., 2010). Another aspect that can be observed from the effect of grafting cycle on ss-CHFM/WSBA is the control of the nano-silica particles grafting uniformity was achieved through layering of the nano-silica particles. Such layer stacks can either lead to a uniform structure on the surface of substrate (Aegerter and Mennig, 2013), as obtained in this study for grafting cycles 3 and 4.

To evaluate the hydrophobic properties of ss-CHFM/WSBA, contact angle measurement was performed on the surface of pristine CHFM/WSBA and grafted ss-CHFM/WSBA as a function of grafting cycle (Fig. 12). As expected, no value of contact angle can be recorded for pristine CHFM/WSBA. Meanwhile, the contact angle values for the grafted ss-CHFM/WSBA showed an increasing trend of 127.5°, 161.1°,

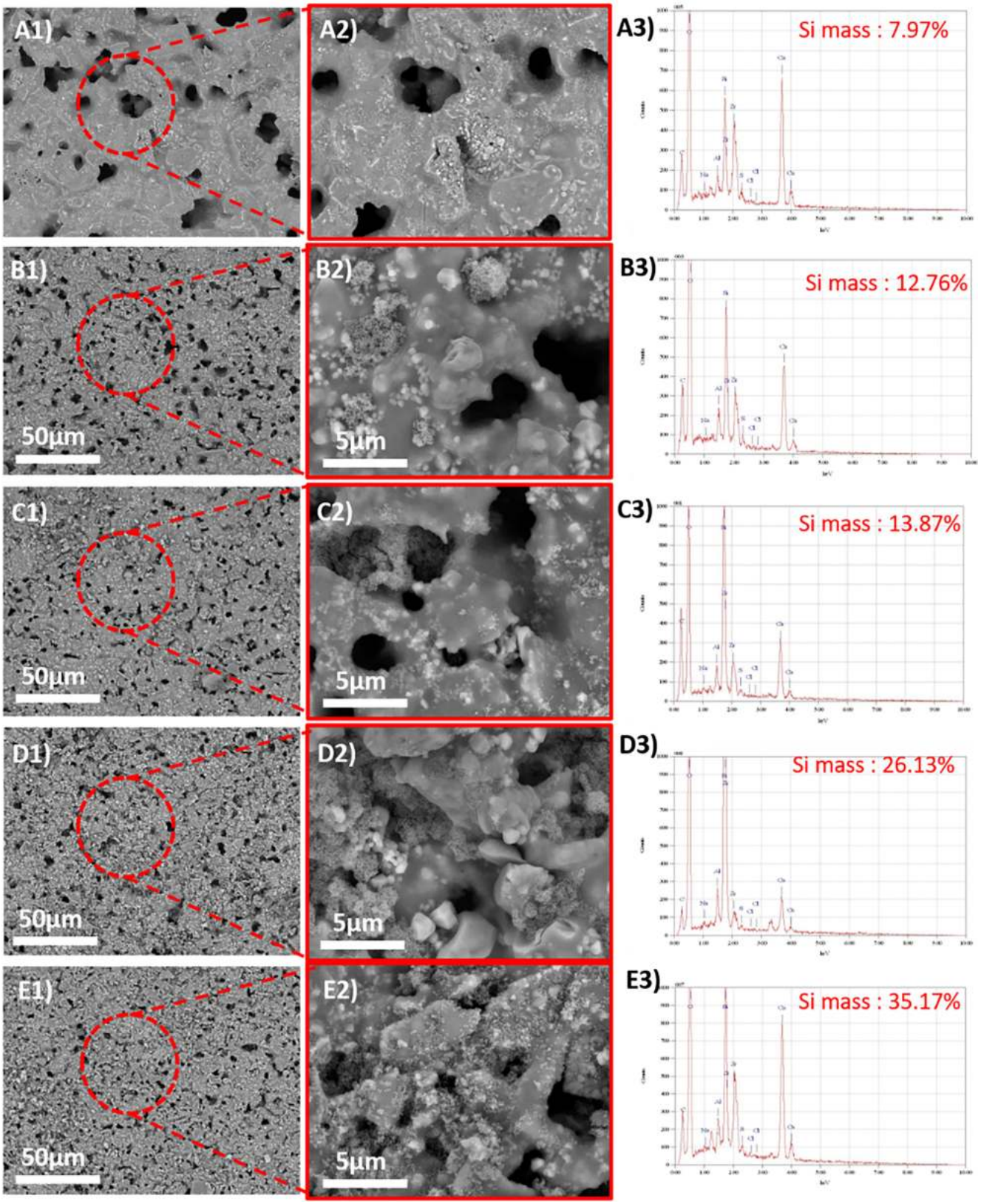

Fig. 10 SEM images of superhydrophobic and superoleophilic CHFM/WSBA grafted for (a) 0 cycle, (b) 1 cycle, (c) 2 cycles, (d) 3 cycles, and € 4 cycles at (1) 1000× and (2) 10,000× magnifications.

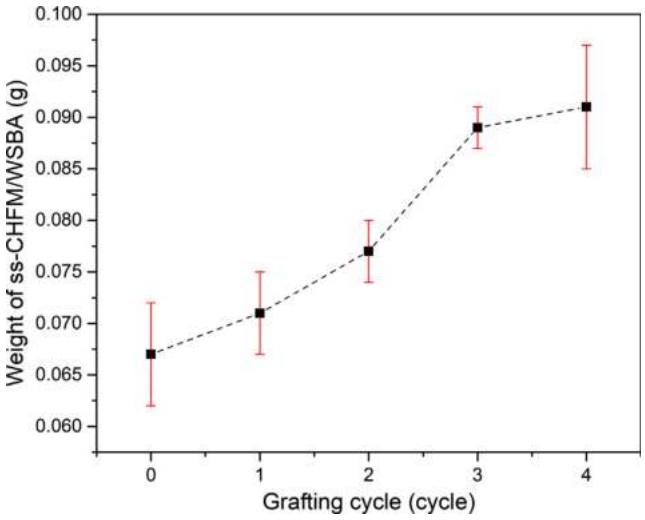

Fig. 11 Weights of pristine CHFM/WSBA and grafted ss-CHFM/WSBA prepared at different grafting cycles.

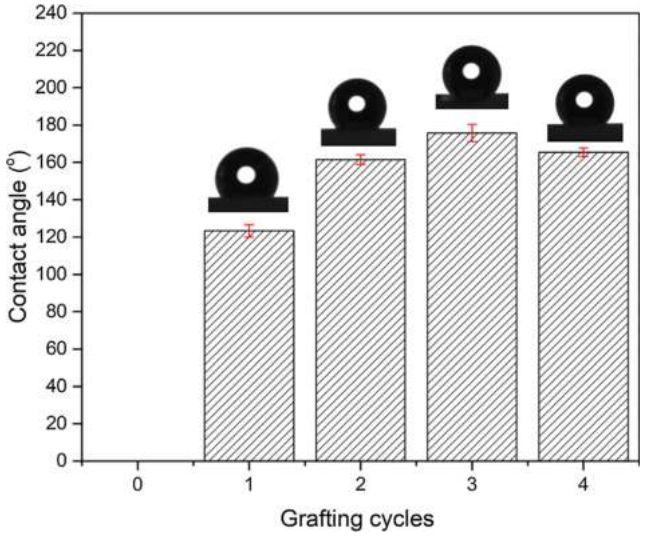

Fig. 12 Contact angle values of ss-CHFM/WSBA prepared at different grafting cycles.

and 173.4° with increasing grafting cycle from 1 to 3 cycles, respectively. The contact angle value dropped to 162.5° when the grafting cycle was increased to 4 cycles. A similar trend was also obtained by Hubadillah et al., explaining that the reduced angle of water droplet is due to the agglomerated silica gels on the membrane surface (Hubadillah et al., 2020). Interestingly, a closed observation revealed that the ss-CHFM/WSBA grafted up to 2 cycles induced superhydrophobic properties where the contact angle value was higher than 150°. This is due to the combination of the nano/micro, hierarchical, and re-entrant structures on the ss-CHFM/WSBA surfaces when grafted via sol–gel method for more than 1 cycle (Ujjain et al., 2016).

The superhydrophobicity and superoleophilicity behaviors of ss-CHFM/WSBA grafted at various grafting cycles were further evaluated towards the oil flux and oil separation efficiency, as presented in Fig. 13. To compare, the performance

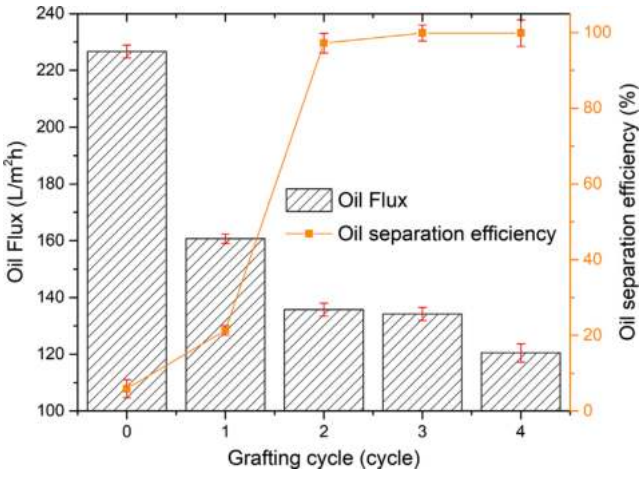

Fig. 13 Performances of ss-CHFM/WSBA prepared at different grafting cycles towards oil separation.

of pristine CHFM/WSBA was also investigated towards oil separation. A similar trend as described previously was observed where no oil flux was recorded for the pristine CHFM/WSBA. Whereas, a decreasing trend was observed for grafted ss-CHFM/WSBA with values of 160.7, 135.7, 134.2, and 120.5 L/m^{2}h for ss-CHFM/WSBA grafted at 1, 2, 3, and 4 cycles, respectively. In terms of oil separation, the permeate solution collected from the pristine CHFM/WSBA contained a mixture of oil and water instead of oil only.

By referring to the Hubadillah et al., this is due to the separation still occurred due to the pores in the pristine membrane (Hubadillah et al., 2017). However, the oil was dominant of being rejected due to the hydrophilicity behavior of the pristine CHFM/WSBA. After grafting at 1 cycle, ss-CHFM/WSBA was able to reject water and 21.3% of oil was collected. Increasing the grafting cycle to 2 cycles increased the oil separation efficiency from 21.3% to 97.2%. Surprisingly, almost only oil (99.9%) was collected from the filtration using ss-CHFM/WSBA grafted for 3 cycles, in which showed that no water penetrated into the pores of ss-CHFM/WSBA. Accordingly, the oil separation efficiency remained when ss-CHFM/WSBA was further grafted for 4 grafting cycles (99.9%).

3.3. Effect of calcination temperature

Calcination is an important process following the hydrophobization of ceramic membrane through sol–gel method. In order to investigate the effect of calcination temperature, ss-CHFM/WSBA prepared at grafting time of 60 min and grafting cycle of 3 times was chosen. Fig. 14 shows the SEM images of ss-CHFM/WSBA calcined at 400, 500, and 600 °C, respectively. A significant change can be observed for the nano-silica particles distribution on the ss-CHFM/WSBA surface when different calcination temperatures were applied. The particles were distributed evenly when calcined at 400 °C. According to Ahmad et al., calcination process was applied to remove the template in the sol and improved the membrane hydrophobicity (Ahmad et al., 2015). In line with this result, de Vos et al. also found that 400 °C was optimum calcination temperature in hydrophobisation of ceramic membrane through sol–gel method with sol containing MTES and found that the

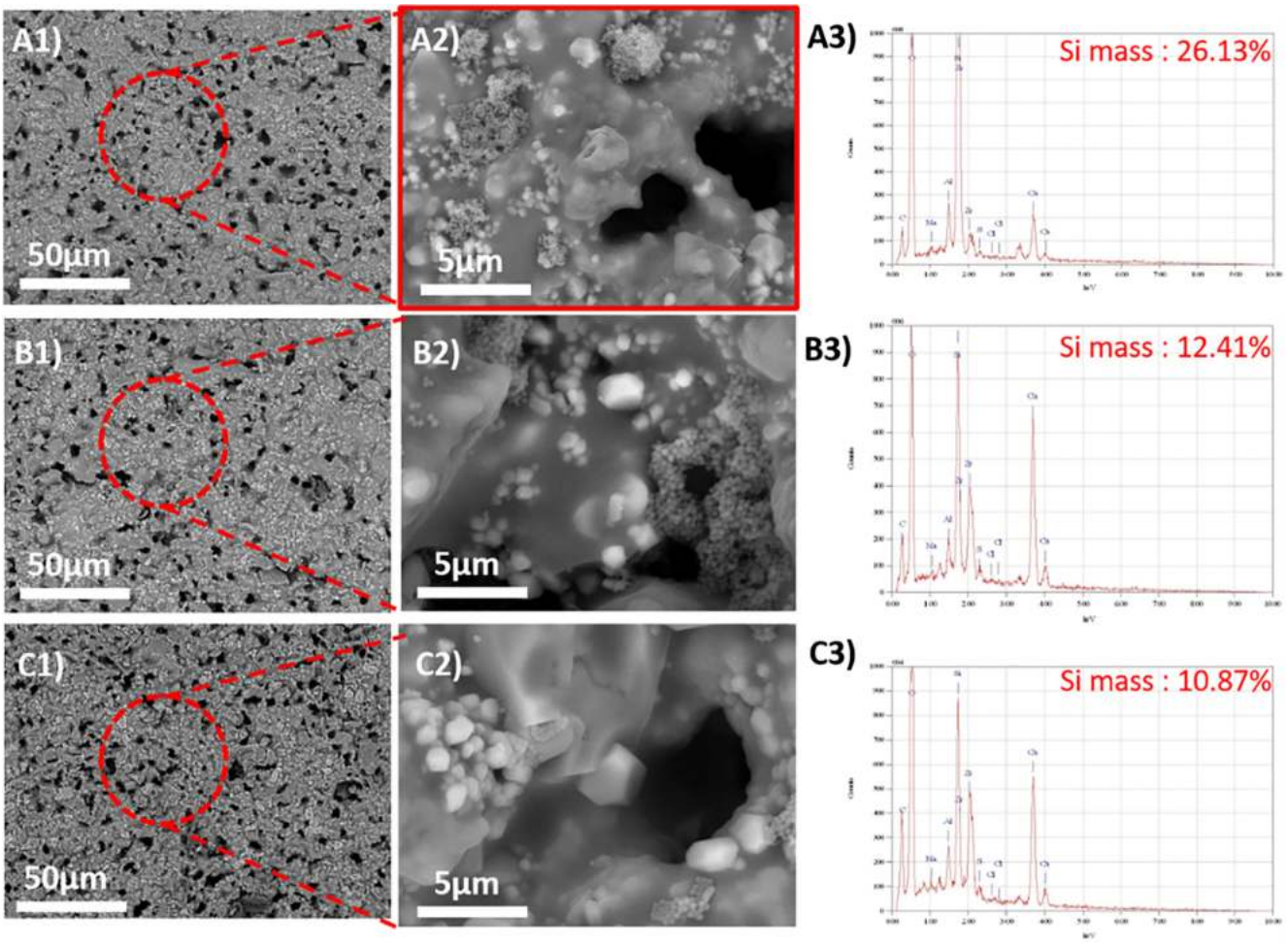

Fig. 14 SEM images of superhydrophobic and superoleophilic CHFM/WSBA grafted at (a) 400 °C, (b) 500 °C, and (c) 600 °C at (1) 1000× and (2) 10,000× magnifications.

hydrophobicity of the ceramic membranes was improved 10 times (de Vos et al., 1999).

Conversely, increasing the calcination temperature from 400 to 500 °C eliminated the nano-silica particles on the ss-CHFM/WSBA surface. At 600 °C, the nano-silica particles disappeared from the ss-CHFMWSBA surface. In addition, a close observation of the SEM images of ss-CHFM/WSBA surface that calcined at 600 °C revealed a smoother surface than that of ss-CHFM/WSBA calcined at 400 °C. This is because at high calcination temperature, the organosilane chain degrades (Ahmad et al., 2015). As a result, the hydrophobicity of the ss-CHFM/WSBA reduced.

To investigate the relationship of calcination temperature and wettability of ss-CHFM/WSBA, contact angle values were measured with water on the surface of ss-CHFM/WSBA calcined at 400, 500, and 600 °C (Fig. 15). As described in Sections 3.1 and 3.2, ss-CHFM/WSBA induced superhydrophobicity properties by having a contact angle value of more than 150° (ss-CHFM/WSBA calcined at 400 °C). However, the contact angle values for ss-CHFM/WSBA dropped from 161.1° (400 °C) to 123.4° and 97.2° for ss-CHFM/WSBA calcined at 500 and 600 °C, respectively. Interestingly, while conducting the contact angle testing on

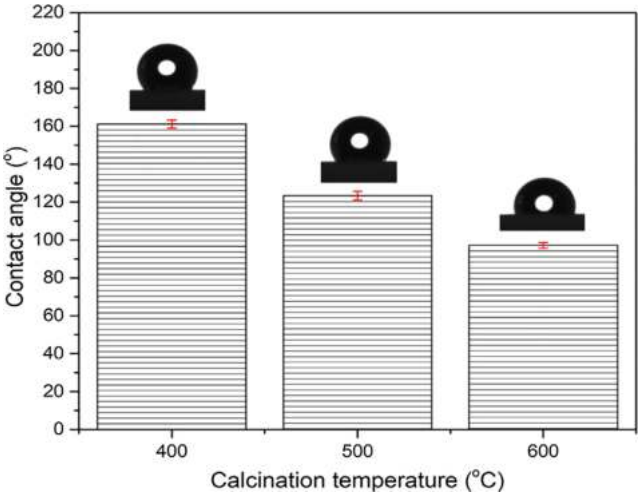

Fig. 15 Contact angle values of ss-CHFM/WSBA prepared at different calcination temperatures.

ss-CHFM/WSBA calcined at 600 °C, it can be observed that the water droplet did not remain static but started to penetrate into the surface of ss-CHFM/WSBA after 10 s (Fig. 16).

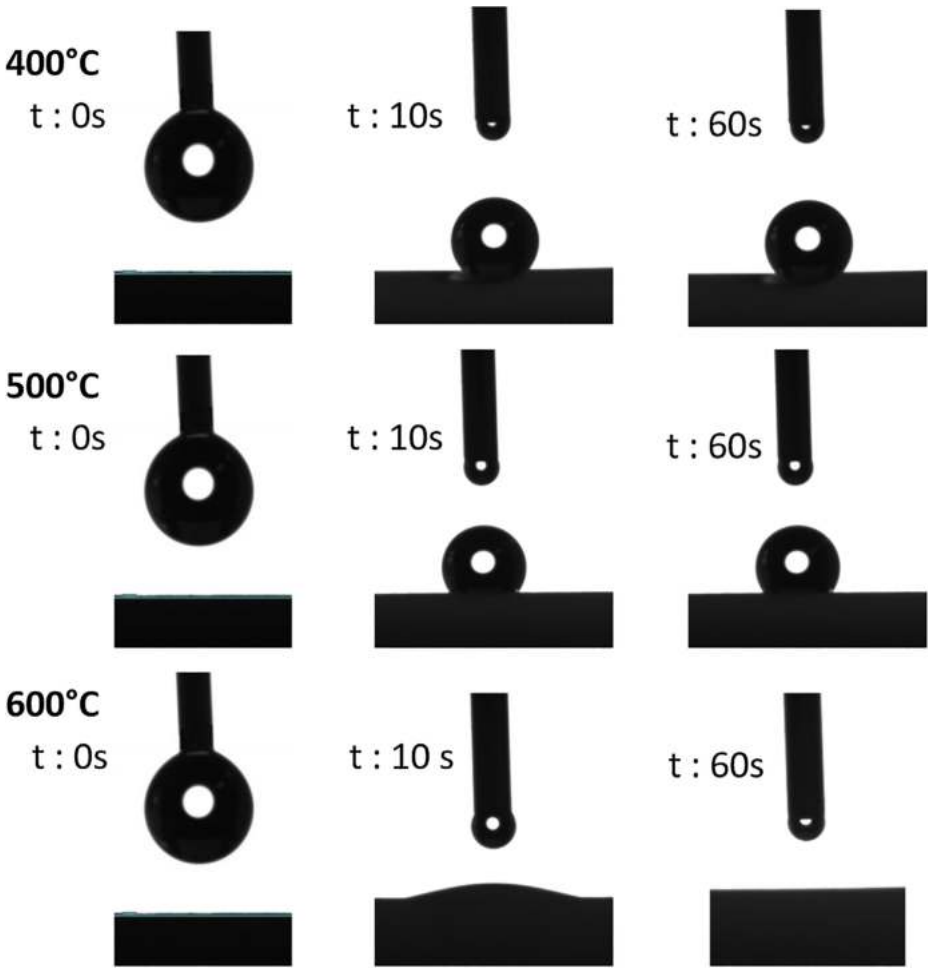

Fig. 16 Water droplet images as a function of time for ss-CHFM/WSBA calcined at various calcination temperatures.

According to Darmawan et al., the methyl group of the silica sol started to oxidize at 500 °C and the surface hydrophobicity was reduced (Darmawan et al., 2018). This finding was supported by Mahadik et al. which reported that the silica layers began losing their hydrophobicity above 550 °C and becoming superhydrophilic at 600 °C due to the oxidation of methyl groups and other organic groups (Mahadik et al., 2010). Budunoglu et al. also reported a similar result for the hydrophobicity and the superhydrophilic layers with contact angle of less than 5° was obtained at 600 °C (Budunoglu et al., 2011), which is in line with the finding obtained in this study.

To investigate the formation of methyl group and other bonds on the CHFM/WSBA surface, FTIR analysis was conducted on the CHFM/WSBA prepared at different calcination temperature and the FTIR spectra are presented in Fig. 17. The peaks of Si—O—Si (1036, 1095, 1108, and 772 cm^{-1}) and Si—OH (1650 cm^{-1}) can be detected. Herein, the peak at 1650 cm^{-1} is due to the bending vibrations of the hydration water, whereas the Si-OH signal generally is visible around 950 cm^{-1} (Catauro et al., 2014). What is most prominent is the Si—C (1275 cm^{-1}) and C—H (2962 cm^{-1}) peaks in the methyl group, showing excellent hydrophobicity (Gui-Long et al., 2011). The intensity of each peak decreased with increasing calcination temperature. For example, the intensity of peak

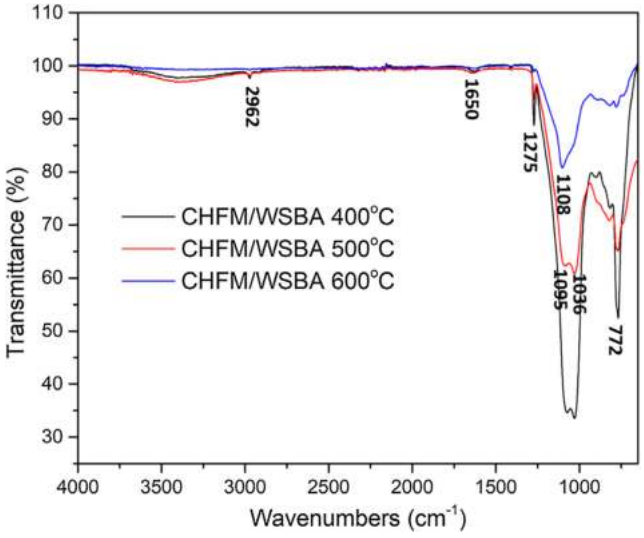

Fig. 17 FTIR spectra for ss-CHFM/WSBA calcined at different temperatures.

of Si—C at 1275 cm^{-1} significantly decreased when the calcination temperature was increased from 400 to 500 °C and totally

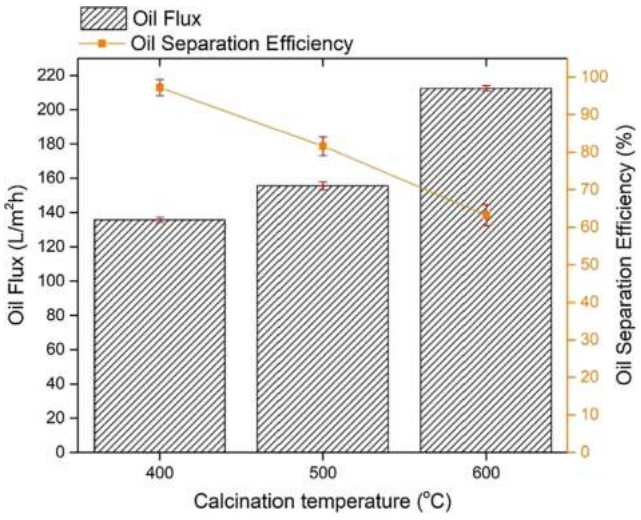

Fig. 18 Performances of ss-CHFM/WSBA prepared at different calcination temperatures towards oil separation.

absent when the calcination temperature was 600 °C. A similar trend was also observed for the C—H peak at 2962 cm^{-1}. This has been explained previously where the methyl group started to oxidize at 500 °C. At this stage, the amount of C—H considerably reduced because of the oxidation process of the C—H group becoming CO_2 (Darmawan et al., 2018).

Fig. 18 presents the performance of ss-CHFM/WSBA at various calcination temperatures towards the oil flux and oil separation efficiency. As expected, the oil flux increased with the increasing calcination temperature and the oil separation efficiency decreased with the increasing sintering temperature. The oil fluxes were 137.2, 160.2, and 216.3 L/m^2h, while the oil separation efficiencies were 99.9%, 80.2%, and 61.3% for ss-CHFM/WSBA calcined at 400, 500, and 600 °C, respectively. The trend can be explained by the distribution of nano-silica particles on the ss-CHFM/WSBA surface. As previously discussed in Fig. 14, ss-CHFM/WSBA calcined at 400 °C showed uniform distribution in which led to the highest oil separation efficiency. The least oil flux obtained was due to the smallest pore size induced by the ss-CHFM/WSBA calcined at 400 °C. Accordingly, as the nano-silica particles on the ss-CHFM/WSBA surface started to decompose, the oil separation efficiency reduced and the oil flux enhanced. However, when the oil flux increased, the water content in the oil collected in the permeate tank was also increased. As a result, the purity of the oil content was poor.

4. Conclusions

In this study, green ceramic hollow fiber membranes derived from sugarcane bagasse waste ash were successfully grafted with superhydrophobic and superoleophilic properties through sol–gel process. To obtain membranes with excellent wettability properties and excellent oil separation performance, three parameters were investigated namely the grafting time (30 to 60 min), grafting cycle (1–4 cycles), and calcination temperature (400–600 °C). The distribution of nano-silica particles grafted on the superhydrophobic and superoleophilic green ceramic hollow fiber membranes were observed through SEM images. It was found that the parameters of sol–gel process gave a significant effect towards the silica distribution on the surface of the grafted membranes.

Depending on grafting time and cycle, agglomeration of nano-silica particles on the membrane surface can be obtained if excessive reaction. As a result, the best superhydrophobic and superoleophilic green ceramic hollow fiber membrane with a contact angle of 161.9° was achieved by grafting at 60 min for 3 cycles and calcined at 400 °C. Consequently, excellent oil flux (134.2 L/m^2h) and oil separation efficiency (99.9%) were obtained.

Acknowledgement

Authors thank to the financial support by Ministry of Higher Education Malaysia (KPT) for Trans-disciplinary Research Grant Scheme (TRGS) vote no. T001, Fundamental Research Grant (FRGS) vote no. 1621 and IGPSU 244.

References

Aegerter, M.A., Mennig, M., 2013. Sol-Gel Technologies for Glass Producers and Users. Springer, US.

Ahmad, N.A., Leo, C.P., Ahmad, A.L., Ramli, W.K.W., 2015. Membranes with great hydrophobicity: a review on preparation and characterization. Sep. Purif. Rev. 44, 109–134.

Budunoglu, H., Yildirim, A., Guler, M.O., Bayindir, M., 2011. Highly transparent, flexible, and thermally stable superhydrophobic ORMOSIL aerogel thin films. ACS Appl. Mater. Interfaces 3, 539–545.

Catauro, M., Bollino, F., Papale, F., Gallicchio, M., Pacifico, S., 2014. Synthesis and chemical characterization of new silica polyethylene glycol hybrid nanocomposite materials for controlled drug delivery. J. Drug Deliv. Sci. Technol. 24, 320–325.

Chen, X., Zhang, J., Wang, Z., Yan, Q., Hui, S., 2011. Humidity sensing behavior of silicon nanowires with hexamethyldisilazane modification. Sens. Actuators, B 156, 631–636.

Crick, C.R., Gibbins, J.A., Parkin, I.P., 2013. Superhydrophobic polymer-coated copper-mesh; membranes for highly efficient oil-water separation. J. Mater. Chem. A 1, 5943–5948.

Darmawan, A., Utari, R., Saputra, R.E., Astuti, Y., 2018. Synthesis and characterization of hydrophobic silica thin layer derived from methyltrimethoxysilane (MTMS). In: IOP Conference Series: Materials Science and Engineering, vol. 299.

de Vos, R.M., Maier, W.F., Verweij, H., 1999. Hydrophobic silica membranes for gas separation. J. Membr. Sci. 158, 277–288.

Dong, Y., Feng, X., Feng, X., Ding, Y., Liu, X., Meng, G., 2008. Preparation of low-cost mullite ceramics from natural bauxite and industrial waste fly ash. J. Alloy. Compd. 460, 599–606.

Feng, X.J., Jiang, L., 2006. Design and creation of superwetting/antiwetting surfaces. Adv. Mater. 18, 3063–3078.

Feng, L., Zhang, Z., Mai, Z., Ma, Y., Liu, B., Jiang, L., Zhu, D., 2004. A super-hydrophobic and super-oleophilic coating mesh film for the separation of oil and water. Angewandte Chem. 116, 2046–2048.

Ge, J., Zhang, J., Wang, F., Li, Z., Yu, J., Ding, B., 2017. Superhydrophilic and underwater superoleophobic nanofibrous membrane with hierarchical structured skin for effective oil-in-water emulsion separation. J. Mater. Chem. A 5, 497–502.

Gui-Long, X., Changyun, D., Yun, L., Pi-Hui, P., Jian, H., Zhuoru, Y., 2011. Preparation and characterization of Raspberry-like SiO2 particles by the sol-gel method. Nanomater. Nanotechnol. 1, 21.

Guo, W., Zhang, Q., Xiao, H., Xu, J., Li, Q., Pan, X., Huang, Z., 2014. Cu mesh's super-hydrophobic and oleophobic properties with

variations in gravitational pressure and surface components for oil/water separation applications. Appl. Surf. Sci. 314, 408–414.
Gupta, S., He, W.-D., Tai, N.-H., 2016. A comparative study on superhydrophobic sponges and their application as fluid channel for continuous separation of oils and organic solvents from water. Compos. B Eng. 101, 99–106.
Harun, Z., Hasan, H.S.K.S., Yunos, M.Z., 2014. Effect of thermodynamic properties on porosity of ceramic membrane prepared by phase inversion. Appl. Mech. Mater. 575, 31–35.
Hedin, A., Johansson, A.J., Lilja, C., Boman, M., Berastegui, P., Berger, R., Ottosson, M., 2018. Corrosion of copper in pure O2-free water? Corros. Sci. 137, 1–12.
Hubadillah, S.K., Harun, Z., Othman, M.H.D., Ismail, A.F., Salleh, W.N.W., Basri, H., Yunos, M.Z., Gani, P., 2016. Preparation and characterization of low cost porous ceramic membrane support from kaolin using phase inversion/sintering technique for gas separation: Effect of kaolin content and non-solvent coagulant bath. Chem. Eng. Res. Des. 112, 24–35.
Hubadillah, S.K., Othman, M.H.D., Harun, Z., Ismail, A.F., Rahman, M.A., Jaafar, J., Jamil, S.M., Mohtor, N.H., 2017. Superhydrophilic, low cost kaolin-based hollow fibre membranes for efficient oily-wastewater separation. Mater. Lett. 191, 119–122.
Hubadillah, S.K., Othman, M.H.D., Matsuura, T., Ismail, A.F., Rahman, M.A., Harun, Z., Jaafar, J., Nomura, M., 2018. Fabrications and applications of low cost ceramic membrane from kaolin: a comprehensive review. Ceram. Int. 44, 4538–4560.
Hubadillah, S.K., Othman, M.H.D., Matsuura, T., Rahman, M.A., Jaafar, J., Ismail, A.F., Amin, S.Z.M., 2018. Green silica-based ceramic hollow fiber membrane for seawater desalination via direct contact membrane distillation. Sep. Purif. Technol. 205, 22–31.
Hubadillah, S.K., Kumar, P., Dzarfan Othman, M.H., Ismail, A.F., Rahman, M.A., Jaafar, J., 2018. A low cost, superhydrophobic and superoleophilic hybrid kaolin-based hollow fibre membrane (KHFM) for efficient adsorption-separation of oil removal from water, RSC. Advances 8, 2986–2995.
Hubadillah, S.K., Othman, M.H.D., Rahman, M.A., Ismail, A.F., Jaafar, J., 2020. Preparation and characterization of inexpensive kaolin hollow fibre membrane (KHFM) prepared using phase inversion/sintering technique for the efficient separation of real oily wastewater. Arabian J. Chem. 13, 2349–2367.
Jamalludin, M.R., Harun, Z., Hubadillah, S.K., Basri, H., Ismail, A. F., Othman, M.H.D., Shohur, M.F., Yunos, M.Z., 2016. Antifouling polysulfone membranes blended with green SiO2 from rice husk ash (RHA) for humic acid separation. Chem. Eng. Res. Des. 114, 268–279.
Jamalludin, M.R., Harun, Z., Othman, M.H.D., Hubadillah, S.K., Yunos, M.Z., Ismail, A.F., 2018. Morphology and property study of green ceramic hollow fiber membrane derived from waste sugarcane bagasse ash (WSBA). Ceram. Int. 44, 18450–18461.
Kingsbury, B.F.K., Li, K., 2009. A morphological study of ceramic hollow fibre membranes. J. Membr. Sci. 328, 134–140.
Koonaphapdeelert, S., Li, K., 2007. Preparation and characterization of hydrophobic ceramic hollow fibre membrane. J. Membr. Sci. 291, 70–76.
Lai, H.Y., Leon, A.D., Pangilinan, K., Advincula, R., 2018. Superoleophilic and under-oil superhydrophobic organogel coatings for oil and water separation. Prog. Org. Coat. 115, 122–129.
Li, B., Liu, X., Zhang, X., Chai, W., 2015. Stainless steel mesh coated with silica for oil–water separation. Eur. Polym. J. 73, 374–379.
Li, J.-J., Zhou, Y.-N., Jiang, Z.-D., Luo, Z.-H., 2016. Electrospun fibrous mat with pH-switchable superwettability that can separate layered oil/water mixtures. Langmuir 32, 13358–13366.
Liu, Y., Zhang, K., Yao, W., Liu, J., Han, Z., Ren, L., 2016. Bioinspired structured superhydrophobic and superoleophilic stainless steel mesh for efficient oil-water separation. Colloids Surf., A 500, 54–63.
Mahadik, S.A., Kavale, M.S., Mukherjee, S.K., Rao, A.V., 2010. Transparent Superhydrophobic silica coatings on glass by sol–gel method. Appl. Surf. Sci. 257, 333–339.
Martínez, C., Cotes, T., Corpas, F.A., 2012. Recovering wastes from the paper industry: development of ceramic materials. Fuel Process. Technol. 103, 117–124.
Obada, D.O., Dodoo-Arhin, D., Dauda, M., Anafi, F.O., Ahmed, A. S., Ajayi, O.A., 2016. Potentials of fabricating porous ceramic bodies from kaolin for catalytic substrate applications. Appl. Clay Sci. 132–133, 194–204.
Song, Y., Liu, Y., Zhan, B., Kaya, C., Stegmaier, T., Han, Z., Ren, L., 2017. Fabrication of bioinspired structured superhydrophobic and superoleophilic copper mesh for efficient oil-water separation. J. Bionic Eng. 14, 497–505.
Tuteja, A., Choi, W., Mabry, J.M., McKinley, G.H., Cohen, R.E., 2008. Robust omniphobic surfaces. Proc. Natl. Acad. Sci. 105, 18200.
Ujjain, S.K., Roy, P.K., Kumar, S., Singha, S., Khare, K., 2016. Uniting Superhydrophobic, Superoleophobic and Lubricant Infused Slippery Behavior on Copper Oxide Nano-structured Substrates. Sci. Rep. 6, 35524.
Vinoth Kumar, R., Kumar Ghoshal, A., Pugazhenthi, G., 2015. Elaboration of novel tubular ceramic membrane from inexpensive raw materials by extrusion method and its performance in microfiltration of synthetic oily wastewater treatment. J. Membr. Sci. 490, 92–102.
Wen, N., Miao, X., Yang, X., Long, M., Deng, W., Zhou, Q., Deng, W., 2018. An alternative fabrication of underoil superhydrophobic or underwater superoleophobic stainless steel meshes for oil-water separation: Originating from one-step vapor deposition of polydimethylsiloxane. Sep. Purif. Technol. 204, 116–126.
Xiang, M., Jiang, M., Zhang, Y., Liu, Y., Shen, F., Yang, G., He, Y., Wang, L., Zhang, X., Deng, S., 2018. Fabrication of a novel superhydrophobic and superoleophilic surface by one-step electrodeposition method for continuous oil/water separation. Appl. Surf. Sci. 434, 1015–1020.
Yang, T., Ma, Z.-F., Yang, Q.-Y., 2011. Formation and performance of Kaolin/MnO2 bi-layer composite dynamic membrane for oily wastewater treatment: Effect of solution conditions. Desalination 270, 50–56.
Yang, H., Pi, P., Cai, Z.-Q., Wen, X., Wang, X., Cheng, J., Yang, Z.-R., 2010. Facile preparation of super-hydrophobic and superoleophilic silica film on stainless steel mesh via sol–gel process. Appl. Surf. Sci. 256, 4095–4102.
Yu, L., Han, M., He, F., 2017. A review of treating oily wastewater. Arabian J. Chem. 10, S1913–S1922.
Zhang, J., Seeger, S., 2011. Polyester materials with superwetting silicone nanofilaments for oil/water separation and selective oil absorption. Adv. Funct. Mater. 21, 4699–4704.
Zhang, L., Zhang, Z., Wang, P., 2012. Smart surfaces with switchable superoleophilicity and superoleophobicity in aqueous media: toward controllable oil/water separation. Npg Asia Mater. 4, e8.
Zhou, Z., Wu, X.-F., 2015. Electrospinning superhydrophobic–superoleophilic fibrous PVDF membranes for high-efficiency water–oil separation. Mater. Lett. 160, 423–427.
Zuo, X., Yu, S., Xu, X., Xu, J., Bao, R., Yan, X., 2009. New PVDF organic–inorganic membranes: The effect of SiO2 nanoparticles content on the transport performance of anion-exchange membranes. J. Membr. Sci. 340, 206–213.